TOPICAL REVIEW — Magnetism, magnetic materials, and interdisciplinary research

Review of magnetic properties and magnetocaloric effect in the intermetallic compounds of rare earth with low boiling point metals*

Ling-Wei Li(李领伟)[1,2,†]

[1] Key Laboratory of Electromagnetic Processing of Materials (Ministry of Education), Northeastern University, Shenyang 110819, China
[2] Institute of Materials Physics and Chemistry, Colleague of Materials Science and Engineering, Northeastern University, Shenyang 110819, China

(Received 21 December 2015; published online 18 January 2016)

The magnetocaloric effect (MCE) in many rare earth (*RE*) based intermetallic compounds has been extensively investigated during the last two decades, not only due to their potential applications for magnetic refrigeration but also for better understanding of the fundamental problems of the materials. This paper reviews our recent progress on studying the magnetic properties and MCE in some binary or ternary intermetallic compounds of *RE* with low boiling point metal(s) (Zn, Mg, and Cd). Some of them exhibit promising MCE properties, which make them attractive for low temperature magnetic refrigeration. Characteristics of the magnetic transition, origin of large MCE, as well as the potential application of these compounds are thoroughly discussed. Additionally, a brief review of the magnetic and magnetocaloric properties in the quaternary rare earth nickel boroncarbides $RENi_2B_2C$ superconductors is also presented.

Keywords: magnetocaloric effect, rare earth based intermetallic compounds, $RENi_2B_2C$ superconductors, magnetic phase transition

PACS: 75.30.Sg, 71.20.Eh, 75.47.Np, 75.50.Ee **DOI:** 10.1088/1674-1056/25/3/037502

1. Introduction of magnetocaloric effect and materials

The magnetocaloric effect (MCE) is a magneto-thermodynamic phenomenon, which was first discovered in pure Fe by Emil Warburg in 1881,[1] and its origin was independently explained by Debye and Giauque in the 1920s.[2,3] All magnetic materials exhibit MCE, although the intensity of this effect depends on the properties of each material. Generally, for a simple ferromagnetic material near its Curie temperature, when a magnetic field is applied, the spins tend to align parallel to the magnetic field, which lowers the magnetic entropy. To compensate for the loss in the magnetic entropy in an adiabatic (isentropic) process, the temperature of the material increases. When the magnetic field is removed, the spins tend to become random which increases the magnetic entropy and the material cools. Meanwhile, Debye and Giauque have also proposed the adiabatic demagnetization in order to achieve temperature lower than that of the liquid helium. This possibility was later experimentally demonstrated by the chemist Nobel Laureate William F. Giauque in 1933, he was able to reach a temperature of 0.25 K based on the adiabatic demagnetization of 61 g paramagnetic salt $Gd_2(SO_4)_3{\cdot}8H_2O$.[4] Besides the success in the ultralow temperature, the magnetic refrigeration technology has also been applied at the higher temperature ranges, such as $\sim$ 2 K to 20 K, the range of liquid helium and hydrogen, as well as $\sim$ 20 K to 80 K, the range of liquid hydrogen and nitrogen.[5–8]

In 1997, two key developments enhanced the feasibility for producing a magnetic refrigerator for commercial or industrial use. The first is that Zimm *et al.*[9] realized the first near room temperature magnetic refrigeration prototype at the Ames Laboratory. The second is that Pecharsky and Gschneider[10] observed a giant MCE in the $Gd_5(Si_2Ge_2)$ compound. Besides the discovery of the giant MCE in $Gd_5(Si_2Ge_2)$ and related compounds,[10,11] a number of materials with giant/large MCE have been realized in the last three decades, for example, $RECo_2$ (*RE* = Er, Ho, and Dy) alloys,[12,13] MnAs based compounds,[14–17] manganites (*RE*, *M*)MnO_3, (*RE* = lanthanide, *M* = Ca, Sr, and Ba),[18,19] Ni–Mn–*X* (*X* = Ga, In, and Sn) based Heusler alloys,[20–24] La(Fe,Si)$_{13}$ and related compounds,[25–28] Mn*TX* (*T* = Co, Ni, and Fe; *X* = Si, Ge) based compounds,[29–32] as well as some rare earth based intermetallic compounds.[33–36] The structure, physical properties, as well as the MCE and its application in most of the above mentioned materials have been summarized in a number of review articles,[11–14,17–19,22,23,26,27,32–35,37–40] which will not be repeated here. In this paper, we give a brief review of our recent progress in exploring magnetocaloric materials, mainly related to several typical systems of *RE*-based intermetallic compounds.

*Project supported by the National Natural Science Foundation of China (Grant Nos. 11374081 and 11004044), the Fundamental Research Funds for the Central Universities, China (Grant Nos. N150905001, L1509006, and N140901001), the Japan Society for the Promotion of Science Postdoctoral Fellowships for Foreign Researchers (Grant No. P10060), and the Alexander von Humboldt (AvH) Foundation (Research stipend to L. Li).

†Corresponding author. E-mail: lingwei@epm.neu.edu.cn

© 2016 Chinese Physical Society and IOP Publishing Ltd

2. Characterization of magnetocaloric materials

2.1. Evaluation of magnetic entropy change and adiabatic temperature change

The MCE is an intrinsic phenomenon for a magnetic material, which manifests as the isothermal magnetic entropy change $\Delta S_{\rm M}$ or/and the adiabatic temperature change $\Delta T_{\rm ad}$ when it is exposed to a varying magnetic field, the definition of $\Delta S_{\rm M}$ and $\Delta T_{\rm ad}$ can be found in Fig. 1. The MCE can be measured directly or it can be calculated indirectly from the experimentally measured heat capacity and/or magnetization. In the present review, the reported values of $\Delta S_{\rm M}$ and $\Delta T_{\rm ad}$ were estimated by two different methods using the indirect technology: (i) from field and temperature dependence of heat capacity $C(H,T)$, (ii) from field and temperature dependence of magnetization $M(H,T)$ and zero field heat capacity $C(T,$ 0 T), which are described as follows.

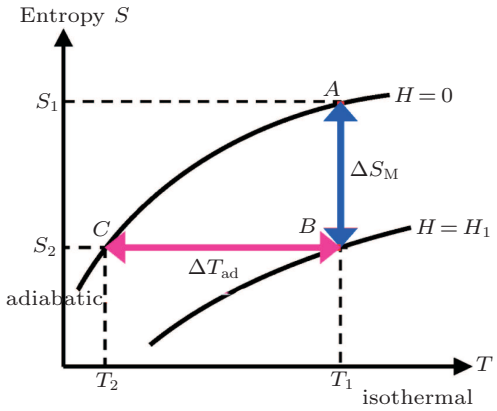


Fig. 1. (color online) The total entropy S as a function of magnetic field H and temperature T, schematically illustrating the definition of the isothermal magnetic entropy change $\Delta S_{\rm M}$ and the adiabatic temperature change $\Delta T_{\rm ad}$.

The temperature dependence of total entropy S under different fields can be calculated from the heat capacity by numerical integration

$$S(H,T)=\int_0^T\left(\frac{C(H,T)}{T}\right)_H {\rm d}T, \tag{1}$$

where H is the magnetic field at which the heat capacity is measured. Then the $\Delta S_{\rm M}$ as well as the adiabatic temperature change $\Delta T_{\rm ad}$ can be calculated from the heat capacity measurements using the following relations:

$$\begin{aligned}\Delta S_{\rm M}(T,\Delta H) &= \int_0^T \frac{C(T,H_1)-C(T,H_0)}{T}{\rm d}T \\ &= [S(T)_{H_1}-S(T)_{H_0}]_T, \qquad (2)\\ \Delta T_{\rm ad}(\Delta H,T) &= [T(S)_{H_1}-T(S)_{H_0}]_S. \qquad (3)\end{aligned}$$

According to the thermodynamical theory, the isothermal magnetic entropy change associated with a magnetic field variation is given by

$$\begin{aligned}\Delta S_{\rm M}(T,\Delta H) &= S_{\rm M}(T,H_1)-S_{\rm M}(T,H_0)\\ &= \int_0^H\left(\frac{\partial S(H,T)}{\partial H}\right)_T {\rm d}H. \qquad (4)\end{aligned}$$

From Maxwell's thermodynamic relation

$$\left(\frac{\partial S(H,T)}{\partial H}\right)_T=\left(\frac{\partial M(H,T)}{\partial T}\right)_H, \tag{5}$$

one can obtain the following expression:

$$\Delta S_{\rm M}(T,\Delta H)=\int_0^H\left(\frac{\partial M(H,T)}{\partial T}\right)_H {\rm d}H, \tag{6}$$

where S, M, H, and T are the magnetic entropy, the magnetization of the material, the applied magnetic field, and the temperature of the system, respectively. From the magnetization measurements made at discrete field and temperature intervals, $\Delta S_{\rm M}$ can be approximately calculated by the following expression:

$$\begin{aligned}&\Delta S_{\rm M}(T,\Delta H)\\ &\approx \frac{1}{\delta T}\left[\int_0^H M(T+\delta T,H)\,{\rm d}H-\int_0^H M(T,H)\,{\rm d}H\right]. \qquad (7)\end{aligned}$$

From zero field $C(T)$, we can calculate S (T, 0 T) by using Eq. (1). With the magnetic entropy change $\Delta S_{\rm M}$ calculated from $M(H,T)$, the $S(T,H)$ can be calculated from the following expression:

$$S(T,H_1)=\Delta S_{\rm M}(T,\Delta H)+\int_0^T\left(\frac{C(T,H_0)}{T}\right)_H {\rm d}T. \tag{8}$$

Then the adiabatic temperature change $\Delta T_{\rm ad}$ can be calculated using Eq. (3). By using the present method, the accuracy of the $\Delta S_{\rm M}$ calculated from the magnetization data for the materials studied here is better than 10%.

2.2. Evaluation of relative cooling power and refrigerant capacity

Another important quality factor(s) for magnetocaloric materials is the relative cooling power (RCP) or/and refrigerant capacity (RC), which is a measurement of the amount of heat transfer between the cold and hot reservoirs in an ideal refrigeration cycle. The RCP is defined as the product of the maximum magnetic entropy change $-\Delta S_{\rm M}^{\rm max}$ and the full width at half maximum $\delta T_{\rm FWHM}$ in the $\Delta S_{\rm M}(T)$ curve,

$${\rm RCP}=-\Delta S_{\rm M}^{\rm max}\times\delta T^{\rm FWHM}. \tag{9}$$

Whereas, the RC is calculated by numerically integrating the area under the $-\Delta S_{\rm M}$–T curve taking the half maximum of the peak as the integration limits

$${\rm RC}=\int_{T_1}^{T_2}|\Delta S_{\rm M}|\,{\rm d}T, \tag{10}$$

where T_1 and T_2 are the temperatures of the cold end and the hot end of an ideal thermodynamic cycle, respectively.

An example for the evaluation of the RCP and RC is displayed in Fig. 2. It is easy to find that the value of RC is around 25 % lower than that of the RCP for the $\Delta S_{\rm M}(T)$ that has a single broad triangle peak around $T_{\rm C}$, which is a typical character for the second order MCE materials.

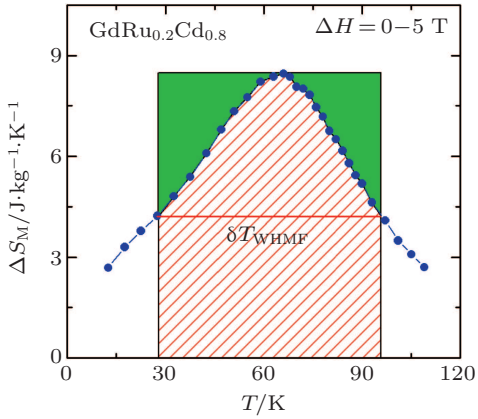


Fig. 2. (color online) Definitions of relative cooling power (RCP) and refrigerant capacity (RC) for $GdRu_{0.2}Cd_{0.8}$. The rectangular area is RCP and the area full with parallel lines is RC.

2.3. Determination of the order of magnetic phase transition

It is well known that the magnitude, temperature, and magnetic field change dependence of MCE have strong correlations with the nature of the corresponding magnetic phase transition; therefore, it is important to determine the order of magnetic transition of the magnetocaloric materials. The Inoue–Shimizu model,[41,42] which involves a Landau expansion of the magnetic free energy up to the sixth power of the total magnetization M, can be used to determine the magnetic transition type,[41,42]

$$F(M,T) = \frac{c_1(T)}{2}M^2 + \frac{c_2(T)}{4}M^4 + \frac{c_3(T)}{6}M^6 + \cdots - BM. \quad (11)$$

After mimimization of the above equation with respect to the magnetization M, the magnetization near the Curie temperature $T_{\rm C}$ satisfies

$$c_1(T)M + c_2(T)M^3 + c_3(T)M^5 = B. \quad (12)$$

The parameters $c_1(T)$, $c_2(T)$, and $c_3(T)$ represent the Laudau coefficients, and it has been reported that the order of a magnetic transition is related to the sign of $c_2(T)$. A transition is expected to be the first order when $c_2(\sim T_{\rm C})$ is negative, whereas it will be the second order for a positive $c_2(\sim T_{\rm C})$. The sign of c_2 can be determined by the Arrott plot (H/M versus M^2 curves),[43] i.e., the magnetic transition is of the second order if all the H/M versus M^2 curves have positive slopes. On the other hand, if the H/M versus M^2 curves show negative slopes, the magnetic transition is of the first order. In the present review, the order of magnetic phase transition of all the materials was determined by this method.

3. MCE in rare earth based intermetallic compounds containing low boiling point metal(s)

The rare earth (*RE*) and transition metal (T) based systems have been intensively investigated in recent years with respect to their interesting chemical and physical properties as well as practical applications in a wide spectrum of industries. Depending on the constituent element and composition, various properties like magnetic ordering, superconductivity, heavy-fermion behavior, valence fluctuation, large magneto-resistance (MR) effect, and large/giant MCE have been observed.[44–48] Compared to the other transition metals, Zn, Mg, and Cd-based intermetallic compounds are less researched. This might be a consequence of the difficulty in material synthesis due to the low boiling point (high vapour pressure) of Zn, Mg, and Cd. Pöttgen *et al.*[49,50] have proposed a simple method to prepare such materials. First, stoichiometric amounts (0.5%–1% of the low boiling point metals were added) of the consistent elementals with purity better than 99.9% were weighted. Second, the weighted metals were arc-welded[49] in a Ta or Nb tube under an argon pressure of ca. 75–85 kPa. The argon was purified over a titanium sponge (900 K), silica gel, and molecular sieves. Third, the crucible was placed in a water-cooled sample chamber of an induction furnace (Hüttinger Elektronik, Freiburg, Germany, Typ TIG 1.5/300)[50] and heated up to a certain high temperature for several minutes, followed by several hours annealing at a selected temperature. Then the obtained samples were ground and cold-pressed into pellets, and finally annealed at a certain temperature for several days in evacuated quartz tubes. The structural properties and phase purity were subsequently characterized by x-ray powder diffraction (XRD) and energy dispersive x-ray spectroscopy (EDX) analyses. In the following sections, our recent progress related to the magnetism and MCE in the binary or ternary intermetallic compounds of *RE* with low boiling point metal(s) (Zn, Mg, and Cd) is reviewed, respectively. For a quick comparison, the magnetic transition temperatures together with the MCE parameters of the compounds in the present review as well as some other rare earth based intermetallic compounds with significant MCE properties are summarized in Table 1.

Table 1. The transition temperature (T_M), the maximum magnetic entropy change ($-\Delta S_M^{max}$), the maximum adiabatic temperature change (ΔT_{ad}^{max}), and the relative cooling power (RCP) under the field changes of 0–2 T and 0–5 T for the intermetallic compounds of rare earth with low boiling point metal(s) (Zn, Mg, and Cd) as well as some giant/large MCE materials with similar T_M. The column with a mark "–" means that the value was not reported in the literature.

Compound	T_M/K	$-\Delta S_M^{max}$/J·kg^{-1}·K^{-1}		RCP/J·kg^{-1}		ΔT_{ad}^{max}/K		Ref.
		2 T	5 T	2 T	5 T	2 T	5 T	
TmZn	8.4	19.6	26.9	76	269	3.3	8.6	[57]
HoZn	26/72	6.5	12.1	255	792	–	–	[58]
EuAuZn	51	4.8	9.1	105	318	–	–	[59]
$EuRh_{1.2}Zn_{0.8}$	95	3.1	5.7	233	513	1.4	2.8	[60]
TmZnAl	2.8	4.3	9.4	53	189	–	–	[61]
Eu_4PdMg	150	2.6	5.5	988	1346	–	–	[66]
Er_4PtMg	15	8.5	17.9	152	483	1.8	4.1	[67]
Er_4PdMg	21	6.2	15.5	142	457	1.7	3.7	[68]
Ho_4PtMg	28	6.1	13.4	177	527	2.2	5.0	[67]
$Gd_2Ni_{0.5}Cu_{1.5}Mg$	57	5.3	9.5	–	688	1.6	3.2	[69]
$Gd_2NiCuMg$	55.2	6.1	11.4	202	630	–	–	[69]
$Gd_4Co_2Mg_3$	77	5.8	–	–	–	1.3	–	[70]
Er_4NiCd	5.9	7.3	18.3	237	595	3.1	7.7	[72]
$GdCd_{0.9}Ru_{0.1}$	149	1.8	4.1	235	636	–	–	[73]
$GdCd_{0.85}Ru_{0.15}$	108	2.4	5.8	223	597	–	–	[73]
$GdCd_{0.8}Ru_{0.2}$	73	3.8	8.5	213	583	–	–	[73]
$ErCr_2Si_2$	1.9	24.1	29.7	136	388	8.4	17.4	[76]
TmAgAl	3.3	7.1	12.4	74	214	–	–	[61]
$GdCr_2Si_2$	4.5	3.1	14.1	35	212	–	–	[77]
ErNiBC	5	17.1	24.8	155	312	5.3	8.6	[78], [79]
$TmMn_2Si_2$	5.5	15.3	22.7	106	250	5.0	10.1	[80]
$ErMn_2Si_2$	6.5	20.0	25.2	130	365	5.4	12.9	[81]
Tm_3Co	8	11.6	19.9	93	300	–	–	[82]
$HoCo_2B_2$	10	6.8	12.2	83	271	–	–	[83]
$DyCo_2B_2$	10	5.4	12.1	88	282	–	–	[83]
ErAgAl	14	4.2	10.5	77	261	–	–	[84]
$TbCo_2B_2$	15	1.5	6.2	49	292	–	–	[83]
GdNiBC	15	9.3	19.8	188	474	4.2	9.9	[78], [85]
HoAgAl	18	3.8	10.3	99	344	–	–	[84]
$DyCo_3B_2$	22	7.4	12.6	154	397	6.4	11.6	[86]
HoPdIn	6/23	7.9	14.6	112	496	2.6	5.5	[87]
$GdCo_2B_2$	25	9.3	17.1	167	462	–	–	[88]
$TbCo_3B_2$	28	4.9	8.7	59	295	4.0	7.3	[89]
$NdMn_2Ge_{0.4}Si_{1.6}$	36	12.3	28.4	95	284	2.1	4.1	[90]
$GdCo_3B_2$	54	5.0	9.4	110	357	2.8	5.2	[91]
ErFeAl	55	2.4	6.1	77	311	–	–	[92]
DyFeSi	70	9.2	17.4	–	–	3.4	7.1	[93]
HoFeAl	80	3.4	7.5	174	563	–	–	[92]
Ho_2In	85	–	11.2	–	360	–	–	[94]
$Gd_{53}Al_{24}Co_{20}Zr_3$ (micro-wire)	96	–	10.3	–	733	–	–	[95]
$Gd_{55}Al_{20}Co_{20}Ni_5$ (metallic glass)	105	6.59	9.8	–	829	–	4.74	[96]
DyFeAl	126	3.1	6.4	190	595	–	–	[97]
Gd_5Ir_2Sn	154	3.9	7.3	176	423	–	–	[98]

3.1. Zn-based intermetallic compounds

The equiatomic binary compounds *RE*Zn with the cubic CsCl-type structure (space group *Pm3m*) have attracted some attention due to their simple crystal structure as well as their interesting physical and chemical properties.[51–54] The magnetic studies revealed that the heavy *RE*Zn compounds order ferromagnetically with the ordering temperature ranging from 267 K for GdZn to 8.5 K for TmZn, whereas the light ones order antiferromagnetically.[51–54] Sousa *et al.*[55,56] have theoretically investigated the MCE in *RE*Zn (*RE* = Tb, Ho, and Er), and some anomalies in $\Delta S_M(T)$ curves were found due to spontaneous and/or spin reorientation transitions in these compounds. Very recently, we have experimentally investigated the magnetic phase transition and magnetocaloric properties of *RE*Zn (*RE* = Tm and Ho) compounds.[57,58]

Figure 3 shows the temperature dependence of the zero field cooling (ZFC) and field cooling (FC) magnetizations (M) for TmZn under various magnetic fields (H) from 0.1 T to 1 T.

Both ZFC and FC $M(T)$ curves show a typical PM to FM transition. With increasing magnetic field, T_C increases gradually from 8.4 K for $H = 0.1$ T to 10.3 K for $H = 1$ T. To evaluate the MCE in TmZn, a set of M(H) curves with increasing and decreasing magnetic field up to 7 T together with the temperature dependence of the heat capacity C for the magnetic field changes of 0–2 T and 0–5 T were measured. No obvious hysteresis can be observed for the whole temperature range. Several isotherms with increasing field are presented in Fig. 4 and the corresponding Arrott plot (H/M versus M^2 curves) is shown in Fig. 5. At the low temperature, the $M(H)$ curve shows the typical behavior of a soft ferromagnet. With the temperature increasing to above 8 K, a field induced metamagnetic transition can be observed in the $M(H)$ curves in a wide temperature range, resulting in a clear S-shape in the Arrott plots, which is a typical characterization of the first-order magnetic phase transition.[43] Additionally, the observed magnetic properties in TmZn are quite similar to those in one of the most important class of MCE materials, $RECo_2$ (RE = Dy, Ho, and Er), which were highlighted due to the occurrence of IEM as well as its close relationship with giant MCE.[12,13]

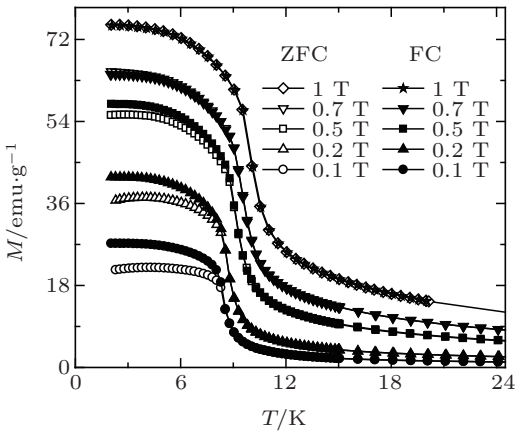


Fig. 3. Temperature dependence of the zero field cooling (ZFC) and field cooling (FC) magnetization (M) for TmZn under various magnetic fields (H) up to 1 T.[57]

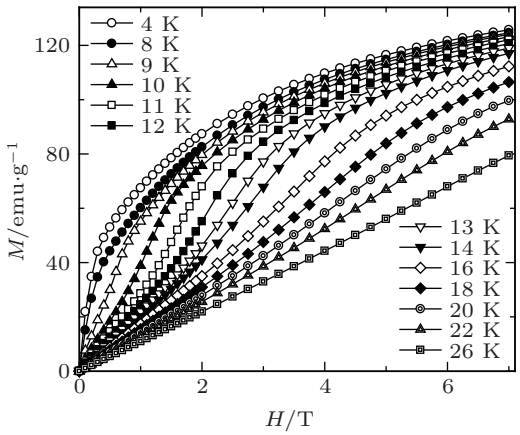


Fig. 4. Magnetic field dependence of the magnetization (increasing field only) for TmZn at some selected temperatures.[57]

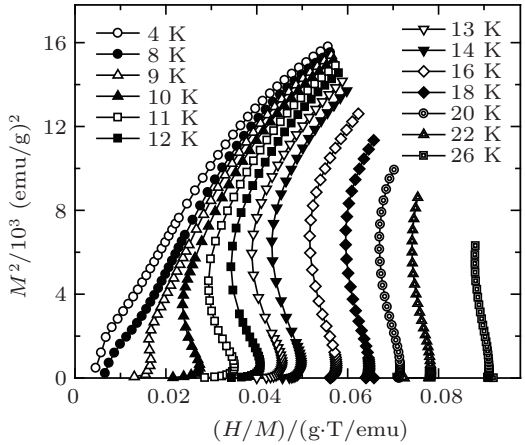


Fig. 5. The plots of H/M versus M^2 for TmZn at some selected temperatures.[57]

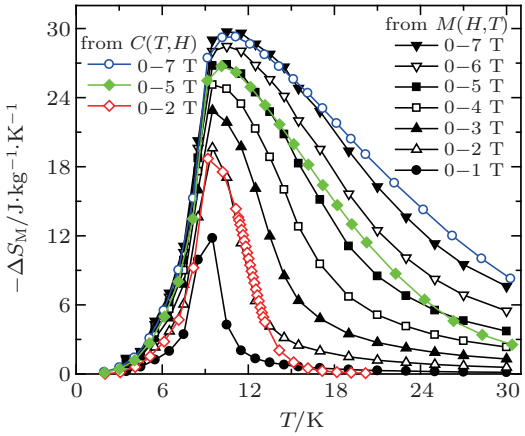


Fig. 6. (color online) Temperature dependence of magnetic entropy change $-\Delta S_M$ for TmZn with the magnetic field changes up to 0–7 T.[57]

The temperature dependences of $-\Delta S_M$ and ΔT_{ad} for TmZn are shown in Figs. 6 and 7, which were calculated from the $M(H,T)$ and $C(T,H)$ data, respectively. Both ΔS_M and ΔT_{ad} obtained by using the two methods described in Section 2 are in good agreement with each other. The values of $-\Delta S_M^{max}$ are 26.9 J/kg·K and 29.7 J/kg·K for the magnetic field changes of 0–5 T and 0–7 T, respectively, and the corresponding values of ΔT_{ad}^{max} are 8.6 K and 11.2 K, indicating that the binary equiatomic compound TmZn belongs to a class of giant magnetocaloric materials. Moreover, for the relatively small field changes of 0–1 T and 0–2 T, the values of $-\Delta S_M^{max}$ reach 11.8 J/kg·K and 19.6 J/kg·K, which is beneficial for applications. The observed giant MCE in TmZn is related to the first order, field-induced metamagnetic phase transition. The field sensitive magnetic transition, sharp changes of magnetization around T_C, and large values of magnetization of TmZn are considered to be the origin of the giant MCE. For the magnetic field changes of 0–2 T, 0–5 T, 0–7 T, the values of RCP and RC are determined to be 76 J/kg, 269 J/kg, 422 J/kg and 59 J/kg, 214 J/kg, 335 J/kg, respectively. The corresponding values of ΔT_{ad}^{max} are estimated to be 3.3 K, 8.6 K, and 11.2 K.[57] These MCE parameters of TmZn (see Table 1), especially for

the magnetic field change of 0–2 T, are comparable to or obviously larger than those of most potential promising magnetic refrigerant materials in the similar temperature region, thus TmZn is attractive for low temperature active magnetic refrigeration.[57]

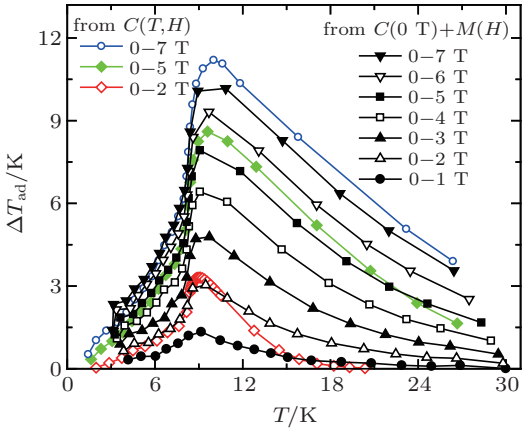


Fig. 7. (color online) Temperature dependence of adiabatic temperature change ΔT_{ad} for TmZn with the magnetic field changes up to 0–7 T.[57]

Whereas, two successive magnetic transitions are observed around $T_{\mathrm{C}} \sim 72$ K and $T_{\mathrm{SR}} \sim 26$ K for HoZn, which are the paramagnetic to ferromagnetic and the spin reorientation transitions, respectively.[58] Magnetization and modified Arrott plots indicate that HoZn undergoes a second-order magnetic phase transition around T_{C}. The critical behavior around T_{C} has been investigated by modified Arrott plots, scaling analysis, scaling plots, and field change dependence on the magnetic entropy change method. The critical exponents β, γ, and δ of HoZn are determined to be 0.47 ± 0.02, 1.09 ± 0.03, and 3.32 ± 0.04, respectively, which have some small deviations from the mean-field theory, indicating a short range or a local magnetic interaction which is properly related to the coexistence of FM and SR transitions at low temperature.[58]

The magnetic entropy change ΔS_{M} for HoZn was calculated from the $M(H,T)$ data (as shown in Fig. 8). One large peak together with a shoulder can be observed in the $-\Delta S_{\mathrm{M}}(T)$ curves around the FM and SR transition temperatures, respectively. Two peaks (shoulder) overlap with each other, resulting in a wide temperature range with a large RCP, which is beneficial for active applications. The maximum magnetic entropy changes ($-\Delta S_{\mathrm{M}}^{\mathrm{max}}$) of HoZn for the magnetic field changes of 0–2 T, 0–5 T, and 0–7 T are 6.5 J/kg·K, 12.1 J/kg·K, and 15.2 J/kg·K, respectively. The corresponding values of RCP are evaluated to be as large as 255 J/kg, 792 J/kg, and 1124 J/kg.[58] These values are obviously larger than those recently reported for potential magnetic refrigerant materials with similar working temperature under the same field changes (see Table 1). The large values of $-\Delta S_{\mathrm{M}}^{\mathrm{max}}$ and RC indicate that HoZn could be a promising candidate for active magnetic refrigeration in the temperature range of 30–90 K.[58]

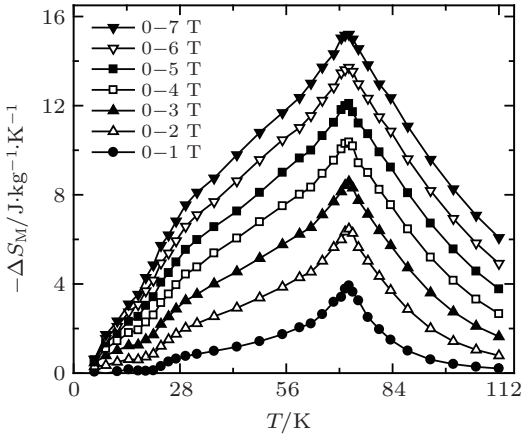


Fig. 8. Magnetic entropy change $-\Delta S_{\mathrm{M}}$ as a function of temperature for various magnetic field changes up to 0–7 T for HoZn.[58]

Hermes *et al.*[59] have studied the magnetic properties and MCE in $EuRh_{1.2}Zn_{0.8}$, which crystallizes with the $MgCu_2$ structure and orders ferromagnetically at $T_{\mathrm{C}} \sim 95$ K. For the magnetic changes of 0–2 T and 0–5 T, the values of $-\Delta S_{\mathrm{M}}^{\mathrm{max}}$, $\Delta T_{\mathrm{ad}}^{\mathrm{max}}$, and RCP are evaluated to be 3.1 J/kg·K and 5.7 J/kg·K, 1.4 K and 2.8 K, and 233 J/kg and 513 J/kg, respectively. A large reversible MCE was reported in EuAuZn around 52 K accompanied by a second order magnetic phase transition from a PM state to an FM state.[60] The values of $-\Delta S_{\mathrm{M}}^{\mathrm{max}}$ in EuAuZn reach 4.8 J/kg·K, 9.1 J/kg·K, and 11.3 J/kg·K for the magnetic field changes of 0–2 T, 0–5 T, and 0–7 T, respectively, and show no thermal and magnetic hysteresis around T_{C}. The corresponding values of $\Delta T_{\mathrm{ad}}^{\mathrm{max}}$ are evaluated to be 2.1 K, 3.8 K, and 4.7 K. Very recently, Zhang *et al.*[61] have reported the magnetic and magnetocaloric properties in the equiatomic intermetallic compounds of TmZnAl. They found that the TmZnAl compound undergoes a second order magnetic transition from PM to FM state around 2.8 K. A reversible MCE with considerable magnitude was observed at low temperature. For the magnetic field changes of 0–2 T, 0–5 T, and 0–7 T, the maximum values of $-\Delta S_{\mathrm{M}}$ are 4.3 J/kg·K, 9.4 J/kg·K, and 11.8 J/kg·K and the corresponding values of RCP (RC) are determined to be 53 (41) J/kg, 189 (149) J/kg, and 289 (228) J/kg, respectively.

3.2. Mg-based intermetallic compounds

The ternary *RE*-rich intermetallic compounds of the general composition $RE_4T\mathrm{Mg}$ (T = Rh, Pd, and Pt), crystallizing in the cubic Gd_4RhIn-type structure, have attracted some attention due to their interesting physical and chemical properties.[62–65] For this type of crystal structure, there are three crystallographically independent *RE* sites and the rare structural motif of Mg_4 tetrahedra. The transition metal atoms are located in RE_6 trigonal prisms with strong covalent *RE*–*T* bonding. These RE_6T basic building units are condensed via common corners and edges to a three-dimensional network in which the cavities are filled by the Mg_4 tetrahe-

dra. Recently, we have reported the magnetic properties and MCE of RE_4PdMg (RE = Eu and Er) and RE_4PtMg (RE = Ho and Er).[66–68] The magnetic phase transition, the origin of the MCE, and its potential application for magnetic refrigeration of these compounds will be shown below.

Figure 9(a) shows the temperature dependent ZFC and FC magnetization M (left scale) and $\mathrm{d}M_{\mathrm{FC}}/\mathrm{d}T$ (right scale) under $H = 0.1$ T for Eu_4PdMg. No difference is observed between the ZFC and FC M–T curves around T_{C}, which is usual in magnetic materials with a second order magnetic transition. Only one peak in $\mathrm{d}M/\mathrm{d}T$ vs. T is observed around 150 K, which is corresponding to the PM to FM magnetic transition. Figure 9(b) shows the FC magnetization M (left scale) and $\mathrm{d}M_{\mathrm{FC}}/\mathrm{d}T$ (right scale) for Eu_4PdMg under $H = 1$ T. We note that M increases continuously with decreasing temperature, and $\mathrm{d}M/\mathrm{d}T$ shows a table-like behavior from 20 K to 150 K.[66] Figure 10 shows the $M(T)$ curves for Eu_4PdMg under various magnetic fields up to 7 T. The magnetic transition is very sensitive to the magnetic field, a sharp PM to FM transition can be observed under a low magnetic field, and the transition gradually becomes broader with increasing magnetic field. The magnetization almost shows a linear temperature dependence under higher magnetic fields. This exotic magnetic transition behavior may be related to its special crystal structure and abundant rare earth site occupation.[66]

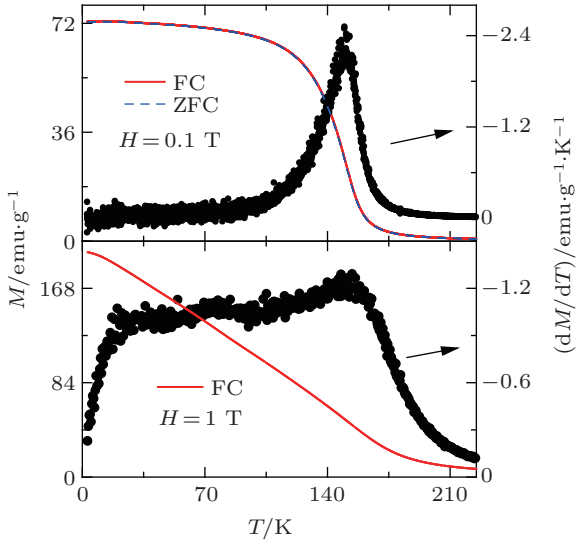


Fig. 9. (color online) (a) Temperature dependence of zero field cooling (ZFC) and field cooling (FC) magnetization M (left scale) as well as $\mathrm{d}M_{\mathrm{FC}}/\mathrm{d}T$ (right scale) for Eu_4PdMg in an external magnetic field $H = 0.1$ T. (b) Temperature dependence of FC magnetization M (left scale) and $\mathrm{d}M_{\mathrm{FC}}/\mathrm{d}T$ (right scale) for Eu_4PdMg under $H = 1$ T.[66]

A set of magnetic isotherms were measured for Eu_4PdMg in the temperature range from 3 K to 220 K to evaluate its magnetic entropy change. No obvious hysteresis can be observed in this temperature range. Additionally, the order of magnetic phase transition in Eu_4PdMg is confirmed to be the second order based on the Banerjee criterion. The resulted $-\Delta S_{\mathrm{M}}(T)$ curves with the magnetic field changes up to 0–7 T are shown in Fig. 11. The $-\Delta S_{\mathrm{M}}(T)$ curves show a pronounced peak around T_{C} for a samll magnetic field change, which is similar to the typical behavior of magnetocaloric materials with a single magnetic phase transition.[66] A very broad table-like behavior can be observed for a high magnetic field change, which is beneficial for application. These peculiar MCE properties in Eu_4PdMg are probably related to the magnetic field sensitive magnetic phase transition and the large saturated magnetic moment which is corresponding to its exotic magnetic and/or crystal structure.[66] With the magnetic field changes of 0–2 T, 0–05 T, and 0–7 T, the values of $-\Delta S_{\mathrm{M}}^{\mathrm{max}}$ are 2.6 J/kg·K, 5.5 J/kg·K, and 7.2 J/kg·K, respectively. The corresponding values of RCP (RC) are determined to be 53 (41) J/kg, 189 (149) J/kg, and 289 (228) J/kg. As a matter of fact, the values of $-\Delta S_{\mathrm{M}}^{\mathrm{max}}$ are smaller than those of recently reported giant MCE materials in the low temperature region, which is related to the additional internal entropy loss due to the larger lattice heat capacity of the material with the higher T_{C}. The $-\Delta S_{\mathrm{M}}^{\mathrm{max}}$ value of Eu_4PdMg is comparable with that of some potential magnetic refrigerant materials in the similar temperature region under the same field change (see Table 1). The RC and RCP values are obviously larger than those of some potential magnetic refrigerant materials in the similar temperature region. The excellent MCE properties indicate that Eu_4PdMg is a promising candidate for active magnetic refrigeration in the 20 K to 160 K temperature range. The present results may also provide an important clue for searching suitable refrigerant materials in the category of materials with field sensitive magnetic phase transition(s).[66]

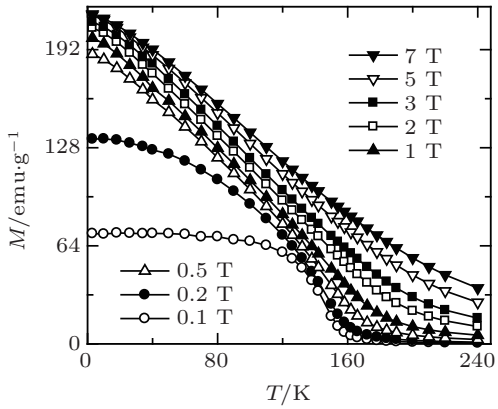


Fig. 10. Temperature dependence of the magnetization for Eu_4PdMg under various magnetic fields up to 7 T.[66]

Very recently, the magnetic properties and MCE in Ho_4PtMg, Er_4PdMg, and Er_4PtMg compounds have been investigated by magnetization and heat capacity measurements.[67,68] The compounds Ho_4PtMg, Er_4PtMg, and Er_4PdMg undergo a second order magnetic phase transition from PM to FM at the Curie temperatures of 28 K, 21 K, and 16 K, respectively. The resulting temperature

dependence of $-\Delta S_{\rm M}$ and $\Delta T_{\rm ad}$ with various magnetic field changes up to 0–7 T for Ho_4PtMg, Er_4PdMg, and Er_4PtMg are shown in Figs. 12(a)–12(c) and 13(a)–13(c), respectively. With the magnetic field changes of 0–1 T, 0–2 T, 0–5 T, and 0–7 T, the values of $-\Delta S_{\rm M}^{\rm max}$ are evaluated to be 2.8 J/kg·K, 6.1 J/kg·K, 13.4 J/kg·K, and 16.9 J/kg·K; 2.8 J/kg·K, 6.2 J/kg·K, 15.5 J/kg·K, and 20.6 J/kg K; and 3.9 J/kg·K, 8.5 J/kg·K, 17.9 J/kg·K, and 22.5 J/kg K for Ho_4PtMg, Er_4PdMg, and Er_4PtMg, respectively, indicating that the presently studied compounds belong to a class of large MCE materials. For the magnetic field changes of 0–2 T, 0–5 T, and 0–7 T, the values of RCP are determined to be 177 J/kg, 527 J/kg, and 762 J/kg; 142 J/kg, 457 J/kg, and 742 J/kg; 152 J/kg, 483 J/kg, and 716 J/kg for Ho_4PtMg, Er_4PdMg, and Er_4PtMg, respectively, and the corresponding values of $\Delta T_{\rm ad}^{\rm max}$ are evaluated to be 1.8 K, 4.1 K, and 5.3 K; 1.7 K, 3.7 K, and 5.5 K; and 2.2 K, 5.0 K, and 6.5 K, respectively. These values are comparable to or even larger than those of some potential promising magnetic refrigerant materials in the similar temperature region, classifying them as potential candidates for low temperature magnetic refrigeration.[67,68]

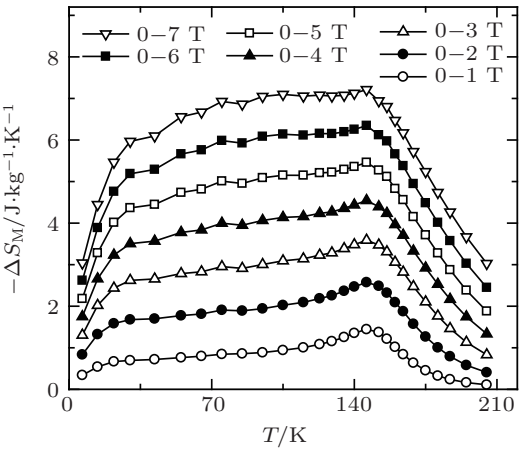


Fig. 11. Temperature dependence of magnetic entropy change $-\Delta S_{\rm M}$ for Eu_4PdMg with the magnetic field changes up to 0–7 T.[66]

Linsinger *et al.*[69] have studied the magnetism and MCE in the $Gd_2Ni_xCu_{2-x}Mg$ ($x = 1$ and 0.5) compounds. Both compounds show a large reversible MCE near their ordering temperatures. The values of $-\Delta S_{\rm M}^{\rm max}$ reach 9.5 J/kg·K and 11.4 J/kg·K for the field change of 0–5 T with no obvious hysteresis loss around 65 K for $x = 0.5$ and $x = 1$, respectively. The corresponding values of RCP reach 688 J/kg and 630 J/kg, which are relatively high compared to those of other MCE materials in that temperature range. These results indicate that $Gd_2Ni_xCu_{2-x}Mg$ could be a promising system for magnetic refrigeration at temperatures below liquid N_2. The values of $\Delta T_{\rm ad}^{\rm max}$ for $Gd_2Ni_{0.5}Cu_{1.5}Mg$ reach 1.6 K and 3.2 K for the magnetic field changes of 0–2 T and 0–5 T, respectively,

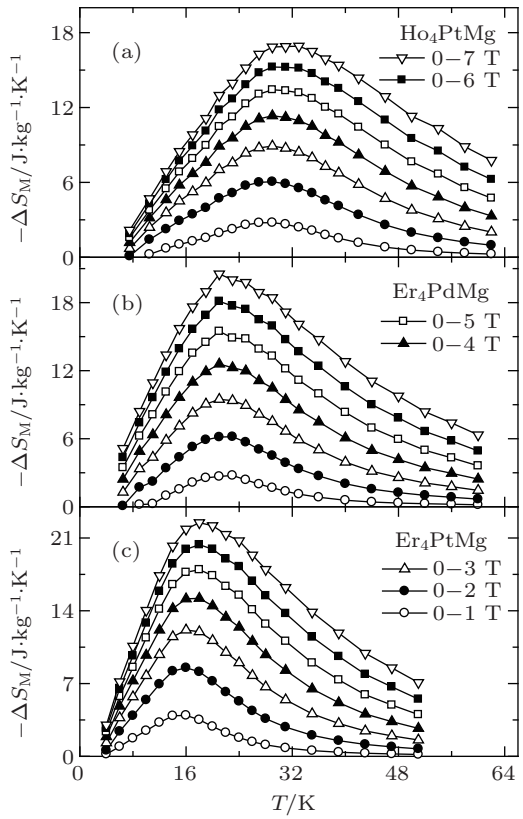


Fig. 12. Temperature dependence of magnetic entropy change $-\Delta S_{\rm M}$ with the magnetic field changes up to 0–7 T for (a) Ho_4PtMg, (b) Er_4PdMg, and (c) Er_4PtMg.[67,68]

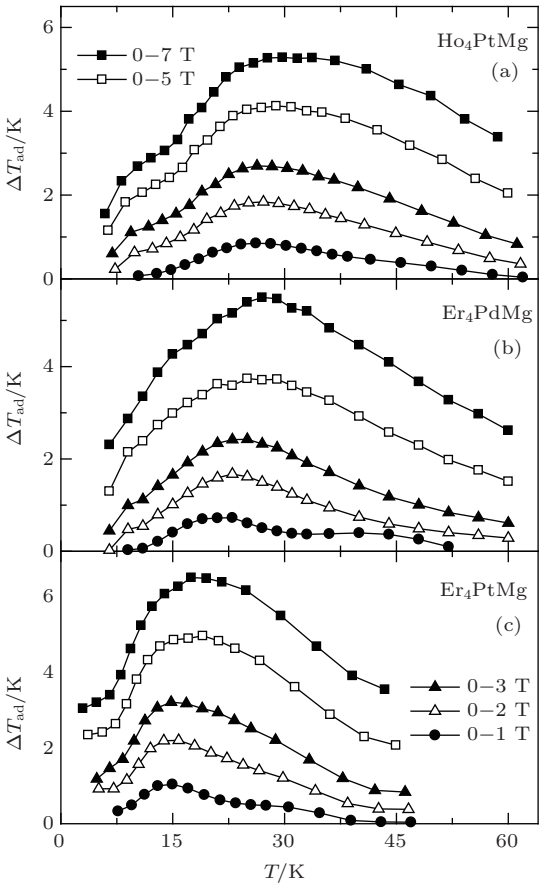


Fig. 13. Temperature dependence of adiabatic temperature change $\Delta T_{\rm ad}$ with the magnetic field changes up to 0–7 T for (a) Ho_4PtMg, (b) Er_4PdMg, and (c) Er_4PtMg.[67,68]

whereas ΔT_{ad}^{max} for $Gd_2NiCuMg$ (1.8 K and 4.3 K) is slightly higher. Gorsse *et al.* have investigated the MCE in the $Gd_4Co_2Mg_3$ compound.[70] They found that the compound orders antiferromagnetically below $T_N = 75$ K and shows a field-induced transition at approximately 0.93 T at 6 K. The values of $-\Delta S_M^{max}$ reach 5.8 J/kg·K and 10.3 J/kg·K at 77 K for the magnetic field changes of 0–2 T and 0–4.6 T, respectively, which is related to the field-induced magnetic phase transition. The corresponding values of ΔT_{ad}^{max} are 1.3(1) K and 3.4(1) K, respectively.

3.3. Cd-based intermetallic compounds

Due to the high toxicity of Cd and its compounds, the Cd-based alloys and compounds have limited technical application, and there is little work on the related topics.[71–73] Hermes *et al.*[72] have investigated the magnetic and MCE properties in the Er_4NiCd compound which crystallizes in the Gd_4RhIn type structure. They found that Er_4NiCd shows a Curie–Weiss behavior above 50 K with $T_N = 5.9$ K. Under a field of 0.4 T, a metamagnetic step is visible, which together with the positive paramagnetic Curie-temperature (7.5 K) indicates a rather unstable antiferromagnetic ground state. The values of ΔS_M^{max} reach −7.3 J/kg·K and −18.3 J/kg·K, and the resulted RCP are 237 J/kg and 595 J/kg, for the magnetic field changes of 0–2 T and 0–5 T, respectively, in Er_4NiCd. The corresponding values of ΔT_{ad}^{max} are 3.1 K and 7.7 K for the magnetic field changes of 0–2 T and 0–5 T, respectively. These results indicate that Er_4NiCd could be a promising system for magnetic refrigeration at temperatures below liquid H_2.[72]

Recently, Li *et al.*[73] have investigated the magnetism and MCE in $GdCd_{1-x}Ru_x$ ($x = 0.1$, 0.15, and 0.2) solid solutions. Figure 14 shows the temperature dependence of ZFC and FC magnetization for $GdCd_{1-x}Ru_x$ under a low magnetic field of $H = 0.1$ T. A typical PM to FM transition can be observed around $T_C \sim 149$ K, 108 K, and 73 K for $x = 0.1$, 0.15, and 0.2, respectively. No obvious thermal hysteresis can be observed between ZFC and FC M–T curves, which is beneficial for application. To evaluate the MCE in $GdCd_{1-x}Ru_x$, a set of $M(H)$ curves around T_C were measured. The resulted temperature dependences of $-\Delta S_M$ for $x = 0.1$, 0.15, and 0.2 are shown in Figs. 15(a)–15(c), respectively. The $-\Delta S_M(T)$ curves show pronounced peaks around T_C, and the peak is getting sharper and the peak temperature gradually shifts to lower temperature with increasing x. Interestingly, a table-like behavior in the $-\Delta S_M(T)$ curve is observed for $x = 0.1$, which is beneficial for application, especially for a single material. For the magnetic field changes of 0–2 T, 0–5 T, and 0–7 T, the values of $-\Delta S_M^{max}$ are evaluated to be 1.8 J/kg·K, 4.1 J/kg·K, and 5.6 J/kg·K; 2.4 J/kg·K, 5.8 J/kg·K, and 7.8 J/kg K; and 3.8 J/kg·K, 8.5 J/kg·K, and 11.0 J/kg K for $x = 0.1$, 0.15, and 0.2, respectively.

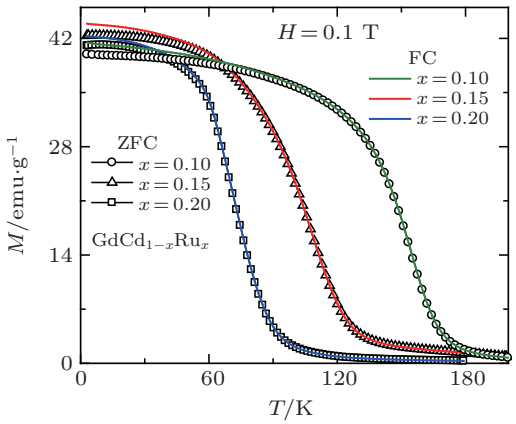


Fig. 14. (color online) Temperature dependence of zero field cooling (ZFC) and field cooling (FC) magnetization M for $GdCd_{1-x}Ru_x$ ($x = 0.1$, 0.15, and 0.2) under a low magnetic field of $H = 0.1$ T.[73]

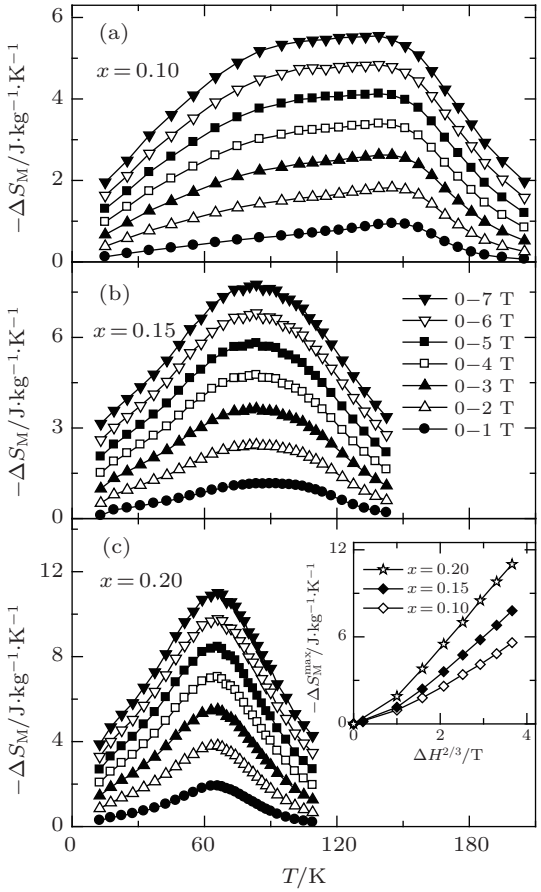


Fig. 15. Temperature dependence of magnetic entropy change $-\Delta S_M$ with various magnetic field changes for $GdCd_{1-x}Ru_x$ ($x = 0.1$, 0.15, and 0.2). The inset shows the maximum magnetic entropy change $-\Delta S_M^{max}$ as a function of magnetic field change $\Delta H^{2/3}$.[73]

The $-\Delta S_M^{max}$ as a function of magnetic field change $\Delta H^{2/3}$ for $GdCd_{1-x}Ru_x$ is shown in the inset of Fig. 15(c). Franco *et al.*[74,75] have previously proposed a universal relation between $-\Delta S_M^{max}$ and ΔH in a magnetic system with second-order phase transition, $-\Delta S_M^{max} \approx A(\Delta H)^n$, where A is a constant. A linear relation between $-\Delta S_M^{max}$ and $(\Delta H)^{2/3}$ can be observed for all the present studied samples under high magnetic field changes, indicating that the critical behavior in

$GdCd_{1-x}Ru_x$ is close to the mean field theory. For the magnetic field changes of 0–5 T and 0–7 T, the values of RCP for $GdCd_{1-x}Ru_x$ are determined to be 636 J/kg, 597 J/kg; 583 J/kg, 889 J/kg; and 852 J/kg, 828 J/kg for $x = 0.1$, 0.15, and 0.2, respectively. Additionally, the $GdCd_{1-x}Ru_x$ solid solution is quite interesting because it can cover a wide temperature range with excellent MCE properties by changing the Ru content, then the materials can be combined to design a composite material used as a magnetic refrigerant. Therefore, the considerable ΔS_M^{max} without any thermal/magnetic hysteresis and large RCP values together with the tunable T_M indicates that the $GdCd_{1-x}Ru_x$ solid solutions are attractive for active magnetic-refrigeration.[73]

4. Magnetic properties and MCE of $RENi_2B_2C$ superconductors

The quaternary rare earth nickel boroncarbides $RENi_2B_2C$, which crystallize in the tetragonal $LuNi_2B_2C$-type structure, have attracted a great deal of attention due to the coexistence of superconductivity and magnetic ordering phenomena.[99–103] The compounds are long range magnetic ordered for RE = Gd, Tb, Dy, Ho, Er, and Tm. The superconductivity is observed for RE = Y, Lu, Dy, Ho, Er, and Tm. Thus, superconductivity coexists with magnetic order for RE = Dy, Ho, Er, and Tm, and the ratio of superconducting transition temperature T_{SC} to antiferromagnetic (AF) ordering temperature T_N ranges from $T_{SC}/T_N = 7.0$ for $TmNi_2B_2C$ to 0.60 for $DyNi_2B_2C$.[101–103] The coexistence and competition of magnetism and superconductivity in these compounds have been systematically investigated experimentally and theoretically.[99–103] In recent years, we have further investigated the MCE in parent and doped $RENi_2B_2C$ superconductors.[104–107] The main achievements will be shown in the following sections. The superconducting transition and the magnetic ordering temperatures together with the MCE parameters are summarized in Table 2 for a quick comparison of the MCE in the $RENi_2B_2C$ superconductors.

4.1. Giant reversible MCE in $Dy_{0.9}Tm_{0.1}Ni_2B_2C$ superconductor

Figure 16 shows the low temperature magnetic isothermals on increasing (open symbols) and decreasing (filled symbols) field for $Dy_{0.9}Tm_{0.1}Ni_2B_2C$ at 2 K and 3 K as well for $DyNi_2B_2C$ at 2 K for a comparison. A large hysteresis for $DyNi_2B_2C$ is observed, in contrast, the hysteresis of $Dy_{0.9}Tm_{0.1}Ni_2B_2C$ is negalectable for $T \geq 3$ K. The magnetic phase transition T_M and superconducting transition temperature T_{SC} are determined to be 9.2 K and 4.5 K, respectively, which are lower than those in $DyNi_2B_2C$.[102,104] A set of selected magnetic isothermals $M(H)$ were measured to evaluate the MCE in $Dy_{0.9}Tm_{0.1}Ni_2B_2C$. The $M(H)$ curves were converted to the Arrot plot of H/M vs. M^2 for $Dy_{0.9}Tm_{0.1}Ni_2B_2C$ at some selected temperatures, which reveals the occurrence of a first order magnetic phase transition based on the Banerjee criterion,[43] as there is a clear S-shaped behavior below the transition temperature.

The resulted magnetic entropy changes $-\Delta S_M$ in $Dy_{0.9}Tm_{0.1}Ni_2B_2C$, which were calculated from $M(H, T)$ curves as a function of temperature, are shown in Fig. 17. The temperature and magnetic field change dependences of the $-\Delta S_M(T)$ curves provide valuable information on the magnetic ordering in $Dy_{0.9}Tm_{0.1}Ni_2B_2C$. For the magnetic field changes $\Delta H \leq 2$ T, $-\Delta S_M$ is negative (inverse MCE) below the transition temperature, and changes to positive with increasing temperature, which is corresponding to the magnetic transition from PM to AFM state. For $\Delta H \geq 3$ T, a positive $-\Delta S_M$ (i.e., conventional MCE) with a broad peak around 13 K is observed. The values of maximum magnetic entropy change $(-\Delta S_M^{max})$ reach 14.7 J/kg·K and 19.1 J/kg·K for the magnetic field changes of 0–5 T and 0–7 T, respectively. The giant MCE

Table 2. The superconductivity transition temperature (T_{SC}), the magnetic transition temperature (T_M), the maximum values of magnetocaloric parameters ($-\Delta S_M^{max}$ and ΔT_{ad}), as well as the relative cooling power (RCP) for the magnetic field change of 0–5 T in the rare earth nickel boroncarbides $RENi_2B_2C$ and $RENiBC$ compounds. The column with a mark "–" means that the value was not reported in the literature. The column with a mark "N" means that superconductivity was not observed above 2 K.

Material	T_{SC}/K	T_M/K	$-\Delta S_M^{max}$/J·kg^{-1}·K^{-1}	ΔT_{ad}^{max}/K	RCP/J·kg^{-1}	Ref.
$Dy_{0.9}Tm_{0.1}Ni_2B_2C$	4.5	9.2	14.7	–	248	[104]
$HoNi_2B_2C$	8.2	5	17.7/19.2	11	283	[105], [106]
$Dy_{0.3}Ho_{0.7}Ni_2B_2C$	8.1	6	18.7	–	264	[106]
$Dy_{0.5}Ho_{0.5}Ni_2B_2C$	6.2	8	18.5	–	275	[106]
$Dy_{0.7}Ho_{0.3}Ni_2B_2C$	6.4	8.5	20.2	–	243	[106]
$DyNi_2B_2C$	6.4	10.5	17.6/17.1	9.7	290	[105], [106]
$DyNi_{1.9}Co_{0.1}B_2C$	N	8.4	16.3	–	309	[107]
$DyNi_{1.9}Co_{0.2}B_2C$	N	8	10.2	–	168	[107]
$DyNi_{1.9}Cr_{0.1}B_2C$	N	9.2	16.1	–	272	[107]
$DyNi_{1.9}Cr_{0.2}B_2C$	N	8.8	13.7	–	219	[107]
$ErNi_2B_2C$	10.5	6.1	11.1/9.8	4.6	155	[105], [108]
$ErNi_{1.9}Fe_{0.1}B_2C$	N	5.6	9.6	–	106	[108]
$ErNi_{1.9}Fe_{0.2}B_2C$	N	5.2	8.0	–	71	[108]

is believed to be related to the field induced first-order magnetic transition from AFM to FM.[104] The field dependence of $-\Delta S_{\rm M}^{\rm max}$ for $Dy_{0.9}Tm_{0.1}Ni_2B_2C$ is also shown in the inset of Fig. 17. The $-\Delta S_{\rm M}^{\rm max}$ increases continuously with the increasing field, and a faster increase of $-\Delta S_{\rm M}^{\rm max}$ with increasing field is observed above 2 T, i.e., the MCE could attain a higher value in a higher magnetic field. The MCE parameters of $Dy_{0.9}Tm_{0.1}Ni_2B_2C$ are comparable with those of the potential promising magnetic refrigerant materials in the similar temperature region.[104]

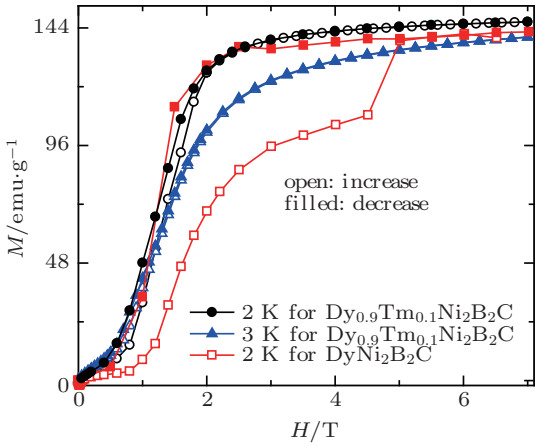


Fig. 16. (color online) Magnetic isothermals on increasing (open symbols) and decreasing (filled symbols) field for $Dy_{0.9}Tm_{0.1}Ni_2B_2C$ at 2 K and 3 K as well for $DyNi_2B_2C$ at 2 K.[104]

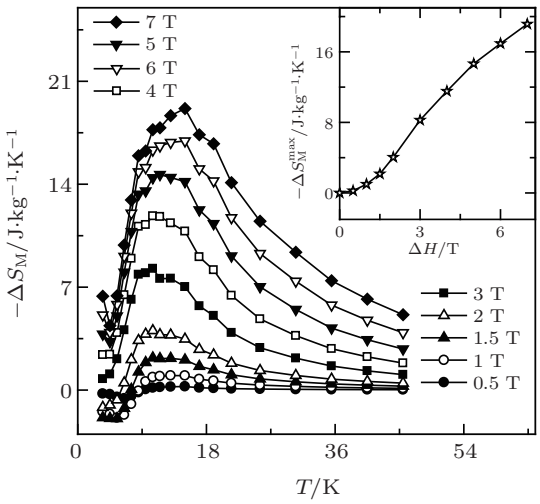


Fig. 17. Temperature dependence of magnetic entropy change $-\Delta S_{\rm M}$ for $Dy_{0.9}Tm_{0.1}Ni_2B_2C$. The inset shows the maximum magnetic entropy change $-\Delta S_{\rm M}^{\rm max}$ as a function of magnetic field changes.[104]

4.2. Large magnetic entropy change in $Dy_{1-x}Ho_xNi_2B_2C$ superconductors

We have also investigated the superconductivity, magnetic properties, and MCE in $Dy_{1-x}Ho_xNi_2B_2C$ ($x = 0$–1) superconductors. The superconducting transition temperature $T_{\rm SC}$ and the magnetic ordering temperature $T_{\rm M}$ are determined to be 6.4 K, 6.4 K, 6.2 K, 8.1 K, 8.2 K and 10 K, 8.5 K, 8 K, 6 K, 5 K for $x = 0$, 03, 0.5, 0.7, 1, respectively.[105,106] A set of selected magnetic isothermals on increasing and decreasing field for $Dy_{1-x}Ho_xNi_2B_2C$ ($x = 0$, 0.3, 0.5, 0.7, and 1) are measured in the temperature range from 2 K to 36 K up to 7 T. Although some hysteresis of $M(H)$ can be observed at low temperatures, it gradually becomes smaller with increasing temperature, and almost disappears above 5 K. All the samples show similar behaviors. Several isotherms with increasing field for $x = 0.5$ are presented in Fig. 18(a). To understand the order of magnetic transition in $Dy_{1-x}Ho_xNi_2B_2C$, the measured M–H isotherms are converted into H/M versus M^2 plots. A clear negative slope in the low temperature and low magnetic field region can be observed for all the compounds, the Arrott plots of $x = 0.5$ are shown in Fig. 18(b) for an example, indicating the first order magnetic phase transition for $Dy_{1-x}Ho_xNi_2B_2C$ ($x = 0$, 0.3, 0.5, 0.7, and 1) compounds.[106]

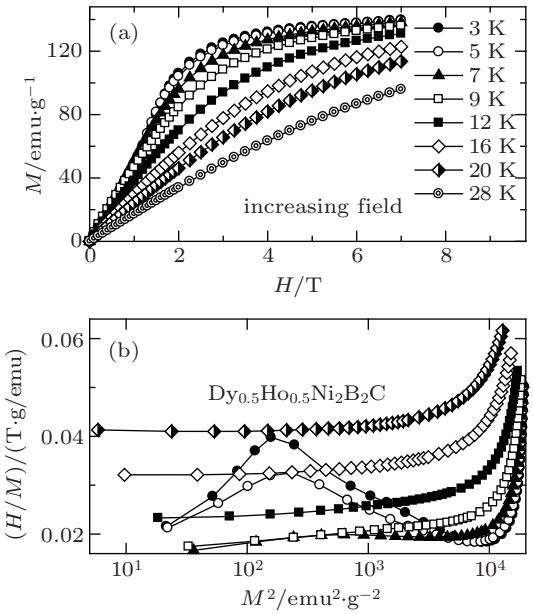


Fig. 18. (a) Magnetic field dependence of the magnetization for $Dy_{0.5}Ho_{0.5}Ni_2B_2C$ at some selected temperatures. (b) The plots of H/M versus M^2 for $Dy_{0.5}Ho_{0.5}Ni_2B_2C$ at some selected temperatures. Copyright (2011) The Japan Society of Applied Physics.[105]

The magnetic entropy change $-\Delta S_{\rm M}$ was calculated from magnetization isotherm $M(H,T)$ curves. The resulted temperature dependence of $-\Delta S_{\rm M}$ is shown in Fig. 19 for $x = 0$, 0.3, 0.7, and 1 and in Fig. 20(b) for $x = 0.5$. The magnetic entropy change for $Dy_{0.5}Ho_{0.5}Ni_2B_2C$ was also calculated from the field and temperature dependence of heat capacity $C(T, H)$ [as shown in Fig. 20(a)] using $\Delta S_{\rm M}(T,\Delta H) = \int_0^T [C(T,H_1) - C(T,H_0)/T]\,{\rm d}T$, and the results are shown in Fig. 20(b). The results of entropy changes calculated from $M(T,H)$ and $C(T,H)$ are consistent with each other. For low magnetic field changes, $-\Delta S_{\rm M}$ is negative (inverse MCE) below the transition temperature, and changes to positive with increasing temperature which can be understood in terms of the FM–AFM phase coexistence and the variation in the ratio of these phases under different magnetic fields. For

the magnetic field changes of 0–5 T and 0–7 T, a positive $-\Delta S_{\rm M}$ (i.e., conventional MCE) with a broad peak can be observed. For the magnetic field changes of 0–2 T, 0–5 T, and 0–7 T, the maximum values of magnetic entropy change ($-\Delta S_{\rm M}^{\rm max}$) are evaluated to be 4.5 J/kg·K, 17.1 J/kg·K, and 22.1 J/kg·K for $x = 0$; 7.3 J/kg·K, 20.2 J/kg·K, and 23.3 J/kg·K for $x = 0.3$; 5.9 J/kg·K, 18.5 J/kg·K, and 22.4 J/kg·K for $x = 0.5$; 6.3 J/kg·K, 18.7 J/kg·K, and 22.9 J/kg·K for $x = 0.7$; and 7.3 J/kg·K, 19.2 J/kg·K, and 22.3 J/kg·K for $x = 1$, respectively.[106] The large magnetic entropy changes in $Dy_{1-x}Ho_xNi_2B_2C$ are believed to be related to the field induced first-order magnetic transition from AFM to FM. The values of RCP are all keeping at the same high values in the range of 45–62 J/kg, 243–290 J/kg, and 414–510 J/kg for the magnetic field changes of 0–2 T, 0–5 T, and 0–7 T, respectively. The values of $-\Delta S_{\rm M}^{\rm max}$ and RCP for $Dy_{1-x}Ho_xNi_2B_2C$ ($x = 0$, 0.3, 0.5, 0.7 and 1) are comparable with those some potential magnetic refrigerant materials reported in the same temperature range, which indicate that the $Dy_{1-x}Ho_xNi_2B_2C$ compounds could be promising candidates for low temperature magnetic refrigeration.[106]

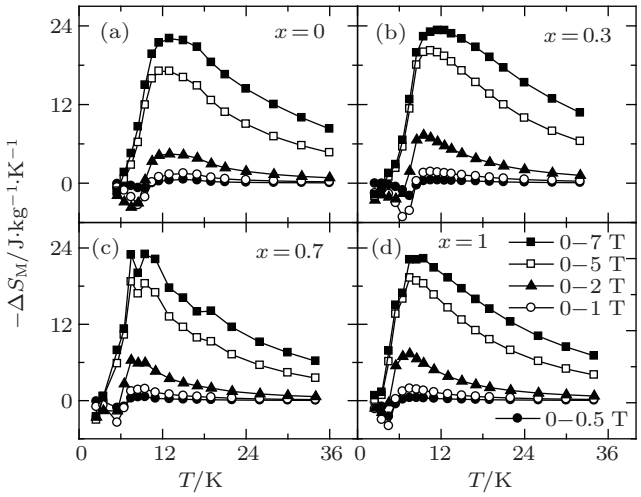


Fig. 19. Temperature dependence of magnetic entropy change $-\Delta S_{\rm M}$ calculated from $M(T,H)$ for $Dy_{1-x}Ho_xNi_2B_2C$ ($x = 0$, 0.3, 0.7, and 1). Copyright (2011) The Japan Society of Applied Physics.[105]

4.3. Ni site doping effect on MCE for $RENi_{2-x}A_xB_2C$ (RE = Dy and Er)

The magnetic properties and MCE of the $DyNi_{2-x}A_xB_2C$ (A = Co and Cr, $x = 0.1$ and 0.2) compounds were also investigated. No superconductivity can be observed above 2 K, and the magnetic transition temperatures $T_{\rm M}$ are determined to be 9.8 K, 8.4 K, 8.0 K, 9.2 K, and 8.8 K for x = 0, 0.1 (Co), 0.2 (Co), 0.1 (Cr), and 0.2 (Cr) in $DyNi_{2-x}A_xB_2C$ system, respectively. Figure 21 shows the magnetic isothermals on increasing (open symbols) and decreasing (filled symbols) field for $DyNi_{2-x}A_xB_2C$ (A = Co and Cr, $x = 0.1$ and 0.2) at 2 K, the hysteresis is neglectable for all the present $DyNi_{2-x}A_xB_2C$, which is beneficial for application. Similar to that of Dy site Tm substitution,[104] Ni site Co or Cr substitution can also effectively reduce (even eliminate) the magnetic hysteresis of $DyNi_2B_2C$.[107]

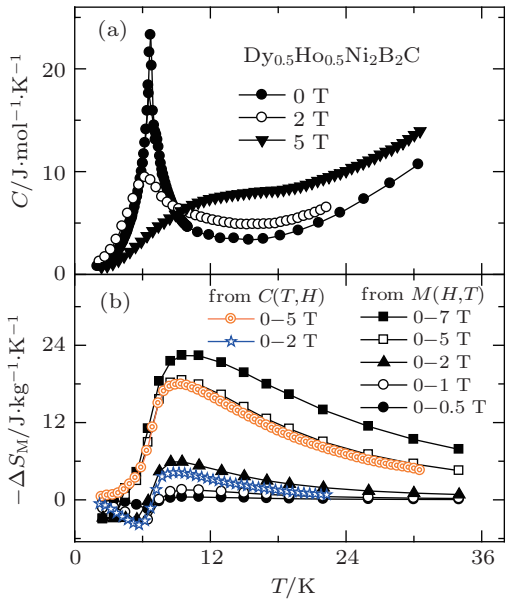


Fig. 20. (color online) (a) Temperature dependence of heat capacity under the magnetic field of 0 T, 2 T, and 5 T for $Dy_{0.5}Ho_{0.5}Ni_2B_2C$. (b) Temperature dependence of magnetic entropy change $-\Delta S_{\rm M}$ for $Dy_{0.5}Ho_{0.5}Ni_2B_2C$ calculated from $C(T, H)$ and $M(T, H)$ respectively. Copyright (2011) The Japan Society of Applied Physics.[105]

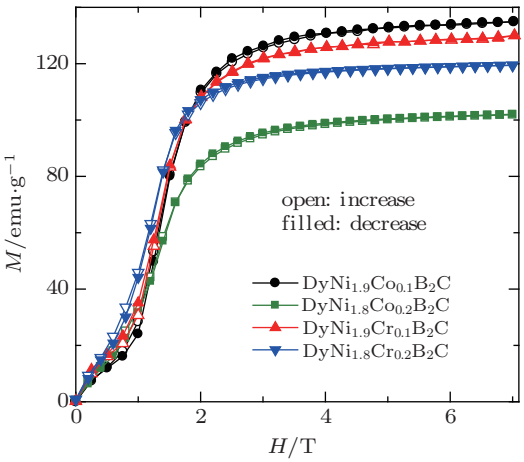


Fig. 21. (color online) Magnetic isothermals on increasing (open symbols) and decreasing (filled symbols) field at 2 K for $DyNi_{2-x}A_xB_2C$ (A = Co and Cr, $x = 0.1$ and 0.2).[107]

To evaluate the MCE in $DyNi_{2-x}A_xB_2C$ (A = Co and Cr, $x = 0.1$ and 0.2), a set of magnetic isothermals were measured. All the samples show similar behaviors. Several isotherms of $DyNi_{1.8}A_{0.2}B_2C$ for A = Co and Cr are presented in Figs. 22(a) and 22(b), and the corresponding Arrott plots are presented in Figs. 22(c) and 22(d). Ni site Co or Cr substitution lowers the magnetic transition temperature $T_{\rm M}$, and reduces the magnetic hysteresis of $DyNi_2B_2C$. A clear negative slope in the low temperature and low magnetic field region can be observed in Figs. 22(c) and 22(d), indicating the first order magnetic phase transition in the $DyNi_{2-x}A_xB_2C$ compounds.

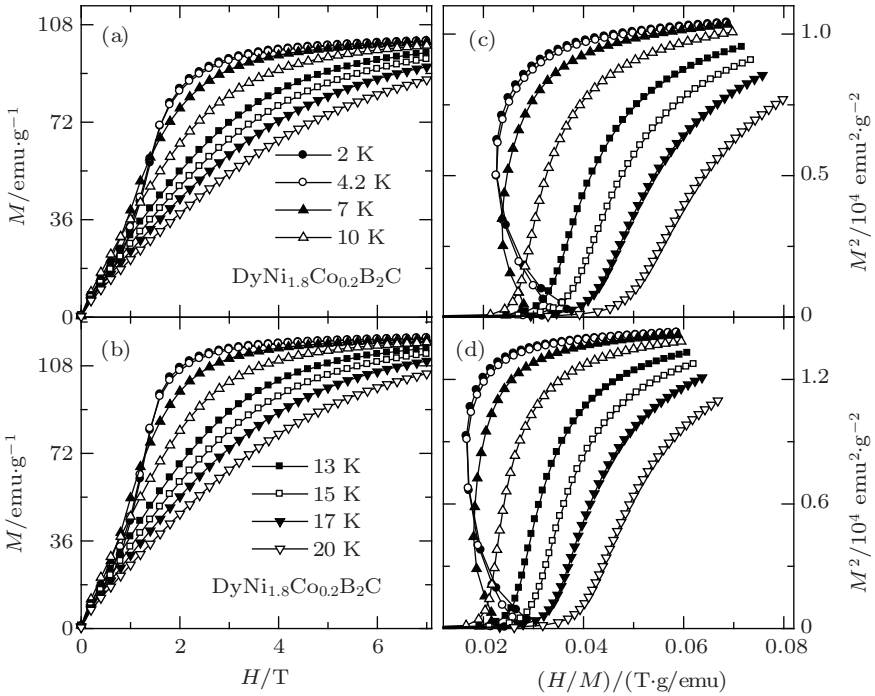


Fig. 22. Magnetic isothermals at some selected temperatures for (a) $DyNi_{1.8}Co_{0.2}B_2C$ and (b) $DyNi_{1.8}Cr_{0.2}B_2C$. The curves of H/M versus M^2 for (c) $DyNi_{1.8}Co_{0.2}B_2C$ and (d) $DyNi_{1.8}Cr_{0.2}B_2C$ at some selected temperatures.[107]

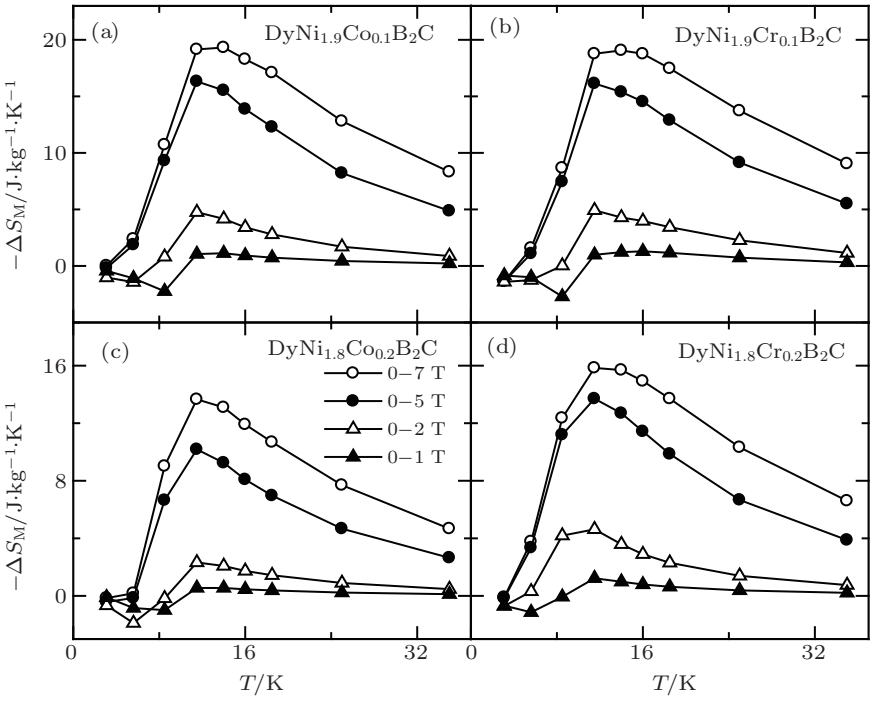


Fig. 23. Temperature dependence of magnetic entropy change $-\Delta S_M$ for $DyNi_{2-x}A_xB_2C$ (A = Co and Cr, $x = 0.1$ and 0.2).[107]

The temperature and field dependences $-\Delta S_M$ for $DyNi_{2-x}A_xB_2C$ (A = Co and Cr, $x = 0.1$ and 0.2) were calculated based on the $M(H,T)$ curves (as shown in Fig. 23). For the magnetic field changes of 0–1 T and 0–2 T, $-\Delta S_M$ is negative (inverse MCE) below the transition temperature, and changes to positive with increasing temperature, for the magnetic field changes of 0–5 T and 0–7 T, a positive $-\Delta S_M$ (i.e., conventional MCE) can be observed. This behavior is similar to that of the $Dy_{1-x}Ho_xNi_2B_2C$ compounds,[106] which can be understood in terms of the FM and AFM phase coexistence and the variation in the ratio of these phases under different magnetic fields. For the magnetic field change of 0–2 T, the minimum and maximum values of $-\Delta S_M$ are evaluated to be -1.4 J/kg·K and 4.7 J/kg·K for $DyNi_{1.9}Co_{0.1}B_2C$, -1.9 J/kg·K and 2.3 J/kg·K for $DyNi_{1.8}Co_{0.2}B_2C$, -1.4 J/kg·K and 4.9 J/kg·K

for $DyNi_{1.9}Cr_{0.1}B_2C$, and -0.7 J/kg·K and 4.6 J/kg·K for $DyNi_{1.8}Cr_{0.2}B_2C$, respectively. The values of $-\Delta S_M^{max}$ are evaluated to be 16.3 J/kg·K, 10.2 J/kg·K, 16.1 J/kg·K, 13.7 J/kg·K and 19.3 J/kg·K, 13.7 J/kg·K, 19.1 J/kg·K, 15.8 J/kg K for $x = 0.1$ (Co), 0.2 (Co), 0.1 (Cr), 0.2 (Cr) in $DyNi_{2-x}A_xB_2C$ for the magnetic field changes of 0–5 T and 0–7 T, respectively.[107]

Zhang and Yang[108] have investigated the magnetic properties and MCE in $ErNi_{2-x}Fe_xB_2C$ ($x = 0$, 0.1, and 0.2) compounds. Similar to those of $DyNi_{2-x}A_xB_2C$ (A = Co and Cr, $x = 0.1$ and 0.2), substitution of Fe for Ni lowers the magnetic transition temperature T_M, and reduces the magnetic hysteresis of $ErNi_2B_2C$. The inverse MCE under low magnetic field at low temperatures is attributed to the nature of antiferromagnetic state for the present $ErNi_{2-x}Fe_xB_2C$ compounds. A normal MCE is observed under higher magnetic field changes, which is related to a field-induced first order metamagnetic transition from AFM to FM state. For the magnetic field change of 0–7 T, the maximum values of magnetic entropy change $-\Delta S_M^{max}$ are 14.5 J/kg·K, 12.7 J/kg·K, and 10.6 J/kg·K for $x = 0$, 0.1 and 0.2 in $ErNi_{2-x}Fe_xB_2C$, respectively.[108]

5. Summary

Investigations of MCE are of great interest for fundamental research and technological application. Our recent progress of the magnetic properties and MCE as well as its origin and potential application for magnetic refrigeration in some rare earth based intermetallic compounds are reviewed, and some of them possess excellent MCE properties. The main achievements are summarized as follows. 1) The TmZn compound exhibits a ferromagnetic state below the Curie temperature of $T_C = 8.4$ K, and processes a field-induced metamagnetic phase transition around and above T_C, resulting in a giant reversible MCE. Particularly, the values of $-\Delta S_M^{max}$ reach 11.8 J/kg·K and 19.6 J/kg·K for low magnetic field changes of 0–1 T and 0–2 T, respectively, indicating that TmZn could be a promising candidate for low temperature and low field magnetic refrigeration. 2) A single-phase Eu_4PdMg compound was synthesised by induction melting of the elements in a sealed tantalum tube in a water-cooled sample chamber. Eu_4PdMg has a very magnetic field sensitive magnetic phase transition, resulting in a reversible, table-like MCE over a broad temperature range. Additionally, the RCP values are obviously larger than those of some potential magnetic refrigerant materials in the similar temperature region, making Eu_4PdMg attractive for magnetic refrigeration from 20 K to 160 K. 3) The $GdCd_{1-x}Ru_x$ solid solutions with $x = 0.1$, 0.15, and 0.2 have been successfully synthesized and the magnetism and MCE have been investigated. The samples undergo a second order magnetic phase transition from a paramagnetic state to a ferromagnetic state at Curie temperatures of $T_C \sim 160$ T, 108 T, and 73 K for $x = 0.1$, 0.15, and 0.2, respectively. A large reversible MCE with a wide temperature range in $GdCd_{1-x}Ru_x$ solid solutions was observed, which makes the $GdCd_{1-x}Ru_x$ solid solutions considerable for active magnetic refrigeration. 4) The Tm substitution effectively reduces the thermal hysteresis of $DyNi_2B_2C$, therefore, a giant reversible MCE has been observed in antiferromagnetic superconductor $Dy_{0.9}Tm_{0.1}Ni_2B_2C$, which is related to a field-induced first order metamagnetic transition from AFM to FM state. 5) The magnetic transition temperature T_M as well as the temperature of $-\Delta S_M^{max}$ in antiferromagnetic superconductors $Dy_{1-x}Ho_xNi_2B_2C$ gradually shifts to low temperature with increasing x, while the values of $-\Delta S_M^{max}$ remain at almost the same high value, which make the $Dy_{1-x}Ho_xNi_2B_2C$ compounds attractive for active magnetic refrigeration at low temperature. The present results may provide some valuable information for searching proper magnetic materials for low temperature magnetic refrigeration.

Acknowledgement

The author sincerely thanks Prof. Rainer Pöttgen from Universität Münster, Germany and Prof. Katsuhiko Nishimura from University of Toyama, Japan for the fruitful discussions and helpful suggestions.

References

[1] Warburg E 1881 *Ann. Phys.* (Leipzig) **13** 141
[2] Debye P 1926 *Ann. Phys.* **81** 1154
[3] Giauque W F 1927 *J. Am. Chem. Soc.* **49** 1864
[4] Giauque W F and MacDougall D P 1933 *Phys. Rev.* **43** 768
[5] Li R, Numazawa T, Hashimoto T, Tomoyiko A, Goto T and Todo S 1986 *Adv. Cryog. Eng.* **32** 287
[6] McMichael R D, Ritter J J and Shull R D J 1993 *Appl. Phys.* **73** 6946
[7] Pecharsky V K and Gschneidner K A Jr 1999 *J. Magn. Magn. Mater.* **200** 44
[8] Tishin A M 1999 *Handbook of Magnetic Materials* **12** 395
[9] Zimm C, Jastrab A, Sternberg A, Pecharsky V K, Gschneidner K Jr, Osborne M and Anderson I 1998 *Adv. Cryog. Eng.* **43** 1759
[10] Pecharsky V K and Gschneidner Jr K A 1997 *Phys. Rev. Lett.* **78** 4494
[11] Gschneidner K A Jr, Pecharsky V K and Tsoko A O 2005 *Rep. Prog. Phys.* **68** 1479
[12] Singh N K, Suresh K G, Nigam A K, Malik S K, Coelho A A and Gama S 2007 *J. Magn. Magn. Mater.* **317** 68
[13] Gratz Z and Markosyan A S 2001 *J. Phys.: Condens. Matter* **3** R385
[14] Bruck E 2005 *J. Phys. D: Appl. Phys.* **38** R381
[15] Tegus O, Bruck E, Buschow K H J and De Boer F R 2002 *Nature* **415** 150
[16] Wada H and Tanabe Y 2001 *Appl. Phys. Lett.* **79** 3302
[17] Yue M, Zhang H G, Liu D M and Zhang J X 2015 *Chin. Phys. B* **24** 017505
[18] Zhong W, Au C K and Du Y W 2013 *Chin. Phys. B* **22** 057501
[19] Phan M H and Yu S C 2007 *J. Magn. Magn. Mater.* **308** 325
[20] Liu J, Gottschall T, Skokov K P, Moore J D and Gutfleisch O 2012 *Nat. Mater.* **11** 620
[21] Li Z, Xu K, Zhang Y, Tao C, Zheng D and Jing C 2015 *Sci. Rep.* **5** 15413
[22] Liu J 2014 *Chin. Phys. B* **23** 047503
[23] Hu F X, Shen B G and Sun J R 2013 *Chin. Phys. B* **22** 037505
[24] Hu F X, Shen B G, Sun J R, Cheng Z H, Rao G H and Zhang X X 2001 *Appl. Phys. Lett.* **78** 3675
[25] Hu F X, Shen B G, Sun J R, Wang G J and Cheng Z H 2002 *Appl. Phys. Lett.* **80** 826

[26] Shen B G, Sun J R, Hu F X, Zhang H W and Cheng Z H 2009 *Adv. Mate.* **21** 4545
[27] Shen B G, Hu F X, Dong Q Y and Sun J R 2013 *Chin. Phys. B* **22** 017502
[28] Fujita A, Fujieda S, Hasegawa Y and Fukamichi K 2003 *Phys. Rev. B* **67** 104416
[29] Zhang C L, Shi H F, Ye E J, Nie Y G, Han Z D, Qian B and Wang D H 2015 *Appl. Phys. Lett.* **107** 212403
[30] Liu E K, Wang W H, Feng L, Zhu W, Li G J, Chen J L, Zhang H W, Wu G H, Jiang C B, Xu H B and Boer de F R 2012 *Nat. Commun.* **3** 873
[31] Wei Z Y, Liu E K, Li Y, Xu G Z, Zhang X M, Liu G D, Xi X K, Zhang H. W, Wang H, Wu G H and Zhang X X 2015 *Adv. Electron. Mater.* **1** 1500076
[32] Wang D H, Han Z D, Xuan H C, Ma S C, Chen S Y, Zhang C L and Du Y W 2013 *Chin. Phys. B* **22** 077506
[33] Zhang H and Shen B G 2015 *Chin. Phys. B* **24** 127504
[34] Franco V, Blazquez J S, Ingale B and Conde A 2012 *Ann. Rev. Mater. Res.* **42** 305
[35] Manosa L, Planes A and Acet M 2013 *J. Mater. Chem. A* **1** 4925
[36] Li L W, Namiki T, Huo D, Qian Z and Nishimura K 2013 *Appl. Phys. Lett.* **103** 222405
[37] Gschneidner K A Jr and Pecharsky V K 2000 *Annu. Rev. Mater. Sci.* **30** 387
[38] Kitanovski A and Egolf P W 2010 *Int. J. Refrig.* **33** 449
[39] Oliveira de N A and Ranke von P J 2010 *Phys. Rep.* **489** 89
[40] Gutfleisch O, Willard M A, E Bruck, Chen C H, Sankar S G and Liu J Ping 2011 *Adv. Mater.* **23** 821
[41] Inoue J and Shimizu M 1982 *J. Phys. F: Met. Phys.* **12** 1811
[42] Liu X B and Altounian Z 2005 *J. Magn. Magn. Mater.* **292** 83
[43] Banerjee B K 1964 *Phys. Lett.* **12** 16
[44] Taylor K N R 1971 *Adv. Phys.* **20** 551
[45] Buschow K H J 1977 *Rep. Prog. Phys.* **40** 1179
[46] Adroja D T and Malik S K 1991 *J. Magn. Magn. Mater.* **100** 126
[47] Kalychak Ya M, Zaremba V I, Pöttgen R, Lukachuk M and Hoffmann R D 2004 *Handbook on the Physics and Chemistry of Rare Earths* **34** 1
[48] Gupta S and Suresh K G 2015 *J. Alloys Compd.* **618** 562
[49] Pöttgen R, Gulden Th and Simon A 1999 *GIT Labor-Fachzeitschrift* **43** 133
[50] Pöttgen R, Lang A, Hoffman R D, Künnen B, Kotzyba G, Müllmann R, Mosel B D and Rosenhahn C 1999 *Z. Kristallogr.* **214** 143
[51] Morin P, Rouchy J and Lacheisserie E T 1977 *Phys. Rev. B* **16** 3182
[52] Galéra R M, Joly Y, Rogalev A and Binggeli N 2008 *J. Phys.: Condens. Matter* **20** 395217
[53] Jeromen A and Trontelj Z 2005 *J. Appl. Phys.* **98** 033515
[54] Givord D, Morin P and Schmitt D 1982 *J. Appl. Phys.* **53** 2445
[55] Sousa de V S R, Plaza E J R and Ranke von P J 2010 *J. Appl. Phys.* **107** 103928
[56] Sousa de V S R, Ranke von P J and Gandra F C G 2011 *J. Appl. Phys.* **109** 063904
[57] Li L W, Yuan Y, Zhang Y, Namiki T, Nishimura K, Pöttgen R and Zhou S 2015 *Appl. Phys. Lett.* **107** 132401
[58] Li L W, Yuan Y, Zhang Y, Pöttgen R and Zhou S 2015 *J. Alloys Compd.* **643** 147
[59] Hermes W, Harmening T and Pöttgen R 2009 *Chem. Mater.* **21** 3325
[60] Li L W, Niehaus O, Gerke B and Pöttgen R 2014 *IEEE Trans. Magn.* **50** 2503604
[61] Zhang Y K, Hou L, Ren Z M, Li X and Wilde G 2016 *J. Alloys Compd.* **565** 635
[62] Kersting M, Matar S F, Schwickert C and Pöttgen R 2012 *Z. Naturforsch.* **67b** 61
[63] Couillaud Y S, Linsinger S, Duée C, Rougier A, Chevalier B, Pöttgen R and Bobet J L 2010 *Intermetallics* **18** 1115
[64] Tappe F, Scheickert C, Linsinger S and Pöttgen R 2011 *Monatsh. Chem.* **142** 1087
[65] Mater S F, Chevalier B B and Pöttgen R 2012 *Intermetallics* **31** 88
[66] Li L W, Niehaus O, Kersting M and Pöttgen R 2014 *Appl. Phys. Lett.* **104** 092416
[67] Li L W, Niehaus O, Kersting M and Pöttgen R 2015 *Intermetallics* **62** 17
[68] Li L W, Niehaus O, Kersting M and Pöttgen R 2015 *IEEE Trans. Magn.* **51** 2503804
[69] Linsinger S, Hermes W, Eul M and Pöttgen R 2010 *J. Appl. Phys.* **108** 043903
[70] Gorsse S, Chevalier B, Tuncel S and Pöttgen R 2009 *J. Solid State Chem.* **182** 948
[71] Tappe F and Pöttgen R 2011 *Rev. Inorg. Chem.* **31** 5
[72] Hermes W, Rodewals U C and Pöttgen R 2010 *J. Appl. Phys.* **108** 113919
[73] Li L W, Niehaus O, Johnscher M and Pöttgen R 2015 *Intermetallics* **60** 9
[74] Franco V, Blázquez J S and Conde A 2006 *Appl. Phys. Lett.* **89** 222512
[75] Franco V, CondeA, Romero-Enrique J M and Blázquez J S 2008 *J. Phys.: Condens. Matter* **20** 285207
[76] Li L W, Hutchison W D, Huo D, Namiki T, Qian Z and Nishimura K 2012 *Scripta Mater.* **67** 237
[77] Li L W, Hu G, Umehara I, Huo D, Hutchison W D, Namiki T and Nishimura K 2013 *J. Alloys Compd.* **575** 1
[78] Li L W, Kadonaga M, Huo D, Qian Z, Namiki T and Nishimura K 2012 *Appl. Phys. Lett.* **101** 122401
[79] Zhang Y K and Wilde G 2015 *Physica B* **472** 56
[80] Li L W, Saensunon B, Hutchison W D, Huo D and Nishimura K 2014 *J. Alloys Compd.* **582** 670
[81] Li L W, Nishimura K, Hutchison W D, Qian Z, Huo D and Namiki T 2012 *Appl. Phys. Lett.* **100** 152403
[82] Mo Z J, Shen J, Yan L Q, Wu J F, Tang C C and Shen B G 2013 *J. Alloys Compd.* **572** 1
[83] Li L W, Nishimura K, Usui G, Huo D and Qian Z 2012 *Intermetallics* **23** 101
[84] Zhang Y K, Yang B J and Wilde G 2015 *J. Alloys Compd.* **619** 12
[85] Zhang Y K and Wilde G 2015 *IEEE Trans. Magn.* **51** 2503104
[86] Li L W, Igawa H, Nishimura K and Huo D 2011 *J. Appl. Phys.* **109** 083901
[87] Li L W, Namiki T, Huo D, Qian Z and Nishimura K 2013 *Appl. Phys. Lett.* **103** 222405
[88] Li L W, Nishimura K and Yamane H 2009 *Appl. Phys. Lett.* **94** 102509
[89] Li L W, Huo D, Igawa H and Nishimura K 2011 *J. Alloys Compd.* **509** 1796
[90] Wang J L, Campbell S J, Cadogan J M, Studer A, Zeng R and Dou S X 2011 *Appl. Phys. Lett.* **98** 232509
[91] Li L W, Nishimura K, Igawa H and Huo D 2011 *J. Alloys Compd.* **509** 4198
[92] Zhang Y K, Wilde G, Li X, Ren Z M and Li L W 2015 *Intermetallics* **65** 61
[93] Zhang H, Sun Y J, Niu E, Yang L H, Shen J, Hu F X, Sun J R and Shen B G 2013 *Appl. Phys. Lett.* **103** 202412
[94] Zhang Q, Cho J H, Li B, Hu W J, Zhang Z D 2009 *Appl. Phys. Lett.* **94** 182501
[95] Bingham N S, Wang H, Qin F, Peng H X, Sun J F, Franco V, Srikanth H and Phan M H 2012 *Appl. Phys. Lett.* **101** 102407
[96] Xia L, Tang M B, Chan K C and Dong Y D 2014 *J. Appl. Phys.* **115** 223904
[97] Li L W, Huo D, Qian Z and Nishimura K 2014 *Intermetallics* **46** 231
[98] Schäfer K, Schwickert C, Niehaus O, Winter F and Pöttgen R 2014 *Solid. State Sci.* **35** 66
[99] Cava R J, Takagi H, Zandbergen H W, Krajewski J J, Peck W F, Siegrist T Jr, Batlogg B, Dover van R B, Felder R J, Mizuhashi K, Lee J O, Eisaki H and Uchida S 1994 *Nature* **367** 252
[100] Canfield P C, Gammel P L and Bishop D J 1998 *Phys. Today* **51** 40
[101] Muller K H and Narozhnyi V N 2001 *Rep. Prog. Phys.* **64** 943
[102] Li L W, Nishimura K, Fujii M, Matsuda K and Huo D 2010 *Phys. Rev. B* **81** 214517
[103] Wolowiec C T, White B D and Maple M B 2015 *Physica C* **514** 113
[104] Li L W and Nishimura K 2009 *Appl. Phys. Lett.* **95** 132505
[105] Li L W, Nishimura K, Huo D, Kadonaga M, Namiki T and Qian Z 2011 *Appl. Phys. Express* **4** 093101
[106] Li L W, Nishimura K, Kadonaga M, Qian Z and Huo D 2011 *J. Appl. Phys.* **110** 043912
[107] Li L W, Fan H, Matsui S, Huo D and Nishimura K 2012 *J. Alloys Compd.* **529** 25
[108] Zhang Y K and Yang B J 2014 *J. Alloys Compd.* **610** 540